ResearchGate

See discussions, stats, and author profiles for this publication at: https://www.researchgate.net/publication/231389892

Simulating the Dynamics of Gas–Solid Flows in a Multichannel Microcirculating Fluidized Bed

ARTICLE *in* INDUSTRIAL & ENGINEERING CHEMISTRY RESEARCH · AUGUST 2009

Impact Factor: 2.59 · DOI: 10.1021/ie8012083

CITATIONS
5

READS
7

3 AUTHORS, INCLUDING:

Faïçal Larachi
Laval University
311 PUBLICATIONS **4,612** CITATIONS

SEE PROFILE

Shantanu Roy
Indian Institute of Technology Delhi
81 PUBLICATIONS **714** CITATIONS

SEE PROFILE

Available from: Shantanu Roy
Retrieved on: 25 January 2016

Simulating the Dynamics of Gas−Solid Flows in a Multichannel Microcirculating Fluidized Bed

Yi-Ning Wang,[†] Faïçal Larachi,*[,†] and Shantanu Roy[‡]

Department of Chemical Engineering, Laval University, Quebec (QC), G1K 7P4, Canada, and Department of Chemical Engineering, Indian Institute of Technology (IIT)—Delhi, New Delhi 110016, India

The dynamics of gas−solid flows and distribution in monolithic multichannel microcirculating fluidized-bed reactors was analyzed using a computational fluid dynamics (CFD) modeling approach. A 2D Euler−Euler multiphase model with the kinetic theory of granular flow has been solved for the detailed monolithic packing geometry. The assemblage of monolithic structured packings with through-flow gas-particulate flows is globally considered in the simulation to capture the dominant mechanisms contributing to the final overall aero/granular dynamics. Due to the complex nature of the interactions between gas and particulate phases and the stationary monolith backbone, one of the challenges in the design and operation of the monolith reactors is the prevention of flow maldistribution. The work presented in this paper forms the basis for a comprehensive reactor-scale model for exploring the intriguing possibilities that the proposed process intensification concept offers for chemical reactions of energy/environmental relevance such as biomass gasification and combustion.

1. Introduction

Biomass is one of the important primary and renewable energy sources. With evidence of depleting fossil fuel sources as well as the evolving global warming issues, the need for utilization of biomass for energy is very promising, particularly because it is believed that energy obtained from biomass has a carbon-neutral cycle. This situation calls for the development of biomass-based but energy-efficient and environment-friendly processes with better environmental acceptability and economic viability.[1,2]

Gasification to produce biosyngas is regarded as one of the most attractive options for biomass conversion and utilization. However, thermodynamics and intrinsic kinetics dictate that endothermic biomass gasification reactions have to be carried out at high temperatures, which demands efficient heat supply and recovery policy. The concept of allothermal gasification offers an attractive solution for implementing high-temperature reactions by coupling strongly endothermic reactions with exothermic reactions.[3] However, implementing the concept in practice is not straightforward.

In the present work, we will first propose an innovative biomass gasification process concept in which the coupling of gasification/combustion process with high-temperature phase-change-material will be implemented in a monolithic structured reactor and intensified by periodic operation mode. To effectively design and optimize this novel process, knowledge from different important fields (including biomass gasification, monolith reactor engineering, high-temperature phase change materials, and fluidized bed reactors) is required. In addition, modeling and understanding of gas−solid (biomass particles) flow hydrodynamics in monolithic structured reactors is very important, in view of the complexity of two-phase flow within such confined microstructured packings. Specifically, due to the complex nature of the interactions between gas and particulate phases and the stationary packing, one of the major challenges in the design and operation of the monolith reactors is prevention of flow *maldistribution*. In order to overcome the limitations posed by this phenomenon, flow distribution characteristics in this type of reactor need to be quantitatively studied and understood. In this work, following the introduction of the novel process concept, the gas−solid two-phase flow distribution characteristics in a monolithic structured reactor have been investigated using a computational fluid dynamics (CFD) simulation approach. A two-dimensional multifluid Euler−Euler CFD model with closure laws according to the kinetic theory of granular flow has been solved. To effectively characterize flow distribution, an assemblage of structured monolithic section with nonstructured packed-bed sections is fully considered in our simulation, allowing comprehensive capture of various possible mechanisms contributing to the final overall aero/granular dynamics. The packed-bed sections are treated as porous media by imposing radial porosity distribution and interphase interactions through user defined functions (UDFs).

2. Hybridization of Gasification/Combustion Processes in Monolithic Structured Reactors

Steam gasification of solid carbonaceous fuels is highly endothermic, which demands input of additional heat to drive reactor conversion. This poses a major challenge because the input of energy reduces the maximum process efficiency. There are a number of potential problems[3] which could be encountered in developing process concepts for biomass gasification with steam: (i) If the biomass is reacted with both air and steam in one reactor, then nitrogen is present in the product stream and is costly to remove. (ii) If one attempts to avoid this problem by using oxygen instead of air, then a source of pure oxygen would be needed, which is again a costly option. (iii) It is possible to circumvent the separation issues by running the "oxygenless" gasification and the combustion reactions in different locations, but then transferring heat from one location to the other is accompanied with heat losses. (iv) Also, in all of these schemes, potential rapid cooling of the product gases leads to tar formation, which adversely affects the process stability and efficiency as well. To avoid this, the product gases

* To whom correspondence should be addressed. Tel.: +1 418 656 3566. Fax: +1 418 656 5993. E-mail: faical.larachi@gch.ulaval.ca.
[†] Laval University.
[‡] Indian Institute of Technology (IIT).

10.1021/ie8012083 CCC: $40.75 © 2009 American Chemical Society
Published on Web 11/19/2008

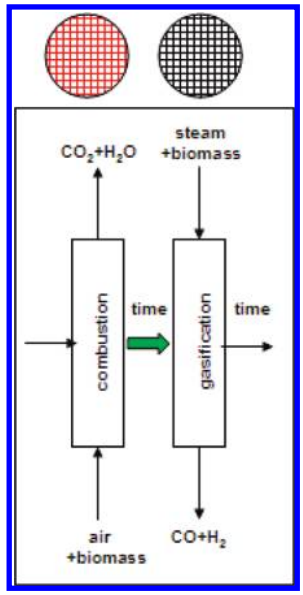

Figure 1. Proposed process concept.

must be kept hot for an optimal duration of their residence time, which allows the tars to crack into lower molecular weight compounds.

In the present work, a process concept which involves time-segregated hybridization of biomass gasification/combustion reactions in a monolithic structured reactor is proposed, as illustrated in Figure 1. In this process, a monolithic microcirculating fluidized bed is used as the reactor unit for gasification/combustion of biomass (Figure 1). At the heart of the proposed process is a monolithic reactor through which gas−solids cocurrent flow occurs, much as in a conventional circulating fluidized bed reactor. However, the presence of the numerous monolith channels serves to segregate the gas−solids flow into these individual cells, which helps to intensify the process. Both the exothermic combustion step and the endothermic gasification step are undertaken in the same monolithic reactor. The process intensification by periodic operation mode is used to temporally segregate the gasification and combustion steps. This is made possible by coating the walls of the monolith channels with high-temperature phase-change-materials (PCMs)[4,5] serving for successive heat storage and heat release in a cyclic operation. The biomass is supplied to the monolithic reactor after fine granulation and subsequent pneumatic conveying. Hence, the process intensification is achieved both by temporal segregation of gasification and combustion as well as the use of a monolithic microfluidized bed reactor with walls coated with PCM. The proposed novel process is supported by the recent advances in (1) the development of microfluidized bed concept for biomass conversion;[6] (2) the development of high-temperature PCM and its application in biomass gasification;[4,5] and (3) the pioneering experimental investigation in flow hydrodynamics of gas−solid two-phase mixture in monolith.[7,8] The proposed concept incorporates the diverse notions proposed by the above referenced papers onto a single platform. Testing the efficacy of the concept through modeling and experimentation is part of our ongoing work and the present contribution is a summary of our first full set of results in addressing a key enabling technology for the concept.

The design and optimization of this novel hybrid process requires accurate understanding of not only the phenomena of biomass thermochemical conversion but also the two-phase hydrodynamics behavior in the monolithic microfluidized reactor which are highly complex in nature. In this regard, the flow distribution characteristics of gas−solids two-phase hydrodynamics in monolithic structured reactor are significantly important for prediction of gasification/combustion performance and examination of strategies for process operation. In the following sections, the development of Euler−Euler CFD multifluid simulation as well as its application for exploring maldistribution of two-phase flow in monolithic packing will be discussed in detail.

3. Representation of Nonuniform Porosity Distribution for Packed-Bed Sections

The reactor computational geometry considered in the present work consists of three sections: an upstream random-packing fixed-bed distributor section, a central monolithic section, and a downstream random-packing fixed-bed section (details are given in section 5). This corresponds to the system geometry reported in the literature by Ding et al.,[7,8] in which the monolith section is sandwiched between the two packed-bed sections. For the fixed-bed randomly packed with solid particles with low D/d_p ratios, the flow is affected by the radial porosity distribution which is a function of the bed diameter (D), particle diameter (d_p), and shape. Therefore, it is essential to define and implement porosity distribution in the simulations to capture the radial distribution characteristics in randomly packed beds. Experimental and computational investigations have shown that for low D/d_p ratio beds the porosity is high near the vicinity of the wall, it oscillates significantly (as a function of radial position) in the near wall region, and typically follows a damped oscillatory function until it reaches a constant value about 5 particle diameters from the wall. Mueller developed a correlation for radial variation of porosity, as a function of particle diameter and bed diameter, which has the following form:[9]

$$\varepsilon(r) = \varepsilon_B + (1-\varepsilon_B)J_0(ar^*)e^{-br} \tag{1a}$$

Where

$$a = \begin{cases} 8.243 - \dfrac{12.98}{(D/d_p - 3.156)} & \text{for } 2.61 \le D/d_p \le 13.0 \\ 7.383 - \dfrac{2.932}{(D/d_p - 9.864)} & \text{for } D/d_p \ge 13.0 \end{cases} \tag{1b}$$

$$b = 0.304 - \frac{0.724}{D/d_p} \tag{1c}$$

$$r^* = \frac{r}{D} \tag{1d}$$

and J_0 is the zeroth-order Bessel function of the first kind. This correlation represents the available experimental data with reasonable accuracy and is widely used. Figure 2 presents the simulated radial porosity variations for our numerical geometry which is characterized by a relatively low column-to-particle ratio $D/d_p = 5$ (i.e., column of 50 mm and packing particles of 10 mm). As compared to the correlation proposed by Giese et al.,[10] Mueller's correlation is adopted in our work since it captures the wall-induced damped oscillations.

4. Eulerian−Eulerian Multifluid Model for Gas−Solid Flow in Monolithic Structured Reactors

An Euler−Euler model with the kinetic theory of granular flow closures is used to model the hydrodynamics of gas−solids flow in the three-section monolithic reactor. The equations employed are a generalization of the Navier−Stokes equations for interacting continua, and all phases are considered to be

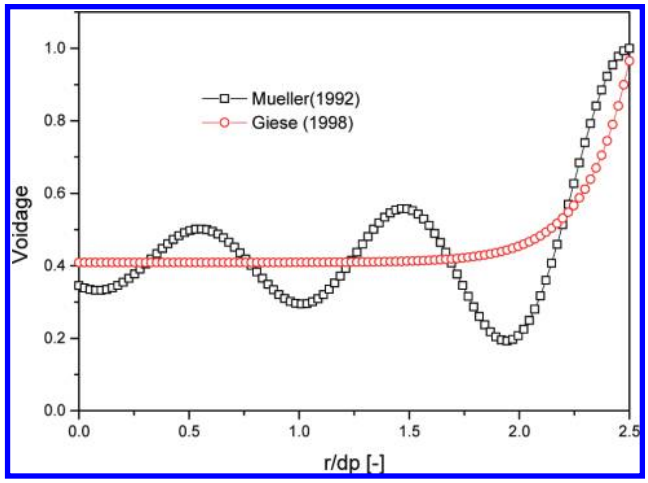

Figure 2. Radial variation of bed porosity in packed-bed sections.

continuous and fully interpenetrating. The governing equations of the model for the gas and solid phases are as follows:

4.1. Continuity and Momentum Conservation Equations. 4.1.1. Mass Conservation Equations of Gas and Particulate Phases. The mass conservation equation for each phase (q = g, s) is described by

$$\frac{\partial}{\partial t}(\rho_q a_q) + \nabla\cdot(\rho_q a_q \vec{v}_q) = 0 \tag{2}$$

Each computational cell is shared by the interpenetrating phases; the sum over all volume fractions is therefore unity:

$$\sum_{q=1}^{N_q} a_q = 1 \tag{3}$$

4.1.2. Momentum Conservation Equations of Gas and Particulate Phases. Momentum conservation for the gas phase is written as

$$\frac{\partial}{\partial t}(a_g\rho_g\vec{v}_g) + \nabla\cdot(a_g\rho_g\vec{v}_g\vec{v}_g) = -a_g\nabla p + \nabla\cdot\bar{\bar{\tau}}_g + a_g\rho_g\vec{g} + \beta_{gs}(\vec{v}_g - \vec{v}_s) + S_g \tag{4}$$

Momentum conservation for the particulate phase can be expressed as

$$\frac{\partial}{\partial t}(a_s\rho_s\vec{v}_s) + \nabla\cdot(a_s\rho_s\vec{v}_s\vec{v}_s) = -a_s\nabla p + \nabla p_s + \nabla\cdot\bar{\bar{\tau}}_s + a_s\rho_s\vec{g} - \beta_{gs}(\vec{v}_g - \vec{v}_s) + S_s \tag{5}$$

where $\bar{\bar{\tau}}_g$ and $\bar{\bar{\tau}}_s$ are the phase stress tensors for gas and solid phases, respectively, and β_{gs} is the drag coefficient between phases.

4.2. Kinetic Theory of Granular Flow Equations. Closure of the particulate phase momentum equation requires constitutive relations for calculating solid pressure, p_s, solid shear viscosity, μ_s, and solid bulk viscosity, λ_s, which can be derived from the granular kinetic theory.[11] The kinetic energy of fluctuation is accounted for by defining a granular temperature, θ_s:

$$\theta_s = \frac{1}{3}\langle v_s'^2\rangle \tag{6}$$

where v_s' is the particulate fluctuating velocity. The granular temperature conservation equation is

$$\frac{3}{2}\left[\frac{\partial}{\partial t}(a_s\rho_s\theta_s) + \nabla\cdot(a_s\rho_s\vec{v}_s\theta_s)\right] = (-p_sI + \bar{\bar{\tau}}_s):\nabla\vec{v}_s + \nabla\cdot(k_{\theta_s}\nabla\theta_s) - \gamma_{\theta_s} \tag{7}$$

where $(-p_sI + \bar{\bar{\tau}}_s):\nabla\vec{v}_s$ is the generation of energy by the solid stress tensor, $\nabla\cdot(k_{\theta_s}\nabla\theta_s)$ is the dispersion of fluctuating kinetic energy in the solids ensemble, and γ_{θ_s} is the collisional dissipation of fluctuating kinetic energy.

The solid pressure, p_s, is composed of a kinetic term that dominates in the dilute flow regions and a collision contribution that is significant in the dense flow region:[11]

$$p_s = a_s\rho_s\theta_s(1 + 2g_0(1 + e_{ss})a_s) \tag{8}$$

where e_{ss} is the coefficient of restitution for particle collisions. The radial distribution function, g_0, is a correction factor that modifies the probability of interparticle collisions.

The solid shear viscosity, μ_s, is calculated by[12,13]

$$\mu_s = \frac{4}{5}a_s\rho_s g_0(1 + e_{ss})\left(\frac{\theta_s}{\pi}\right)^{1/2} + \frac{10\rho_s d_s\sqrt{\theta_s\pi}}{96a_s(1 + e_{ss})g_0}\times\left[1 + \frac{4}{5}g_0a_s(1 + e_{ss})\right]^2 \tag{9}$$

The solids bulk viscosity, λ_s, is expressed as[11]

$$\lambda_s = \frac{4}{3}a_s\rho_s d_s g_0(1 + e_{ss})\sqrt{\frac{\theta_s}{\pi}} \tag{10}$$

4.3. Closure Relationships for Interphase Interactions. The interaction coefficient between the gas phase and flowing particulate phase can be described by a combination of Wen and Yu[14] and Ergun[15] equations. The final drag coefficient for this combination is expressed as

$$\beta_{gs} = \begin{cases} \beta_{Ergun} = \dfrac{3}{4}C_D\dfrac{a_s a_g\rho_g|\vec{v}_s - \vec{v}_g|}{d_s}a_g^{-2.65} & a_g \geq 0.8 \\ \beta_{Wen-Yu} = 150\dfrac{a_s^2\mu_g}{a_g d_s^2} + 1.75\dfrac{a_s\rho_g}{d_s}|\vec{v}_s - \vec{v}_g| & a_g < 0.8 \end{cases} \tag{11}$$

The drag coefficient C_D is evaluated by

$$C_D = \begin{cases} \dfrac{24}{a_g Re_s}[1 + 0.15(a_g Re_s)^{0.687}] & Re_s < 1000 \\ 0.44 & Re_s \geq 1000 \end{cases} \tag{12}$$

with the Reynolds number based on the solids−gas relative velocity, Re_s, defined by

$$Re_s = \frac{\rho_g d_s|\vec{v}_s - \vec{v}_g|}{\mu_g} \tag{13}$$

To avoid discontinuity between the two equations, Gidaspow[13] introduced a switch function that gives a smooth but rapid transition from one regime to the other:

$$\varphi_{gs} = \frac{\arctan[150\times 1.75\times(0.2 - a_s)]}{\pi} + 0.5 \tag{14}$$

Thus, the interaction coefficient between fluid particle phases is finally expressed as

$$\beta = (1 - \varphi_{gs})\beta_{Ergun} + \varphi_{gs}\beta_{Wen-Yu} \tag{15}$$

The interaction between the gas phase and the stationary packing phase, i.e., lower and upper packed bed sections, can be expressed using an Ergun-type equation:[15]

$$S_g = \frac{150\mu_g}{d_p^2}\frac{(1 - \varepsilon)^2}{\varepsilon^2}a_g^2\vec{v}_g + \frac{1.75\rho_g}{d_p}\frac{(1 - \varepsilon)}{\varepsilon}a_g^3\vec{v}_g^2 \tag{16}$$

In the literature, there are a few attempts made to evaluate the interaction force between powder and packing particle

phases.[16−18] In this work, the interaction between the flowing suspended phase and the stationary packing phase is expressed by[17,19]

$$S_s = -\frac{1}{2D^*}\rho_s(\varepsilon a_s)\left|\frac{\vec{U}_s}{a_s}\right| f_k\left(\frac{\vec{U}_s}{a_s}\right) \tag{17}$$

Where

$$f_k = \frac{14.98}{Fr^{1.33}} \tag{18}$$

$$D^* = \frac{2d_p(1-\varepsilon)}{3\varepsilon} \tag{19}$$

$$Fr = \frac{|\vec{U}_s|}{\sqrt{D^* g}} \tag{20}$$

where $\vec{U}_s = \vec{v}_s \cdot (a_s\varepsilon)$ is the superficial suspended solids velocity vector.

4.4. Definition of Maldistribution Quantities. To quantify the flow nonuniformity of two-phase flow distribution in each channel, the flow factor, Γ_i^q (defined as the ratio of the actual flow rate through the channel to the theoretical flow rate that would exist in the corresponding channel for the case of uniform distribution[20]), is used here:

$$\Gamma_i^q = \frac{\dot{m}_i^q}{\dot{m}_{i,0}^q} \tag{21}$$

where $\dot{m}_i^q$ denotes the mass flowrate of the qth phase in the ith channel in an actual (potentially maldistributed) flow field, while $\dot{m}_{i,0}$ is the theoretical flowrate of the qth phase in the ith channel, assuming uniform flow distribution. In practice, the value of Γ_i^q may be *greater than* or *less than* 1.0, representing a *flow excess* or *flow starvation* state in each channel, respectively.

Besides the flow factor, the maldistribution factor, M_f, which was first introduced by Hoek et al.[21] and modified by Marcandelli et al.,[22] is also adopted in this work to determine the flow distribution over the entire cross-section of the monolith block:

$$M_f^q = \sqrt{\frac{1}{N_{ch}(N_{ch}-1)}\sum_i (\Gamma_i^q - 1)^2} \tag{22}$$

where N_{ch} is the number of channels. M_f^q equals 0.0 when the flow is distributed uniformly; and M_f^q approaches 1.0 when the flow is highly selective to one single channel.

5. Computational Geometry, Boundary Conditions, and Numerical Solution

The monolith geometry reported in the literature by Ding et al.[7,8] is considered in our simulation, which has a length of 600 mm and a (square) cell size of 3 mm (cell size represents clearance without cell wall thickness); see Table 1. As far as the cold unit simulations are concerned, this selected block length is judged representative for highlighting the gas and solids flow maldistribution issues. Should it be necessary and depending on the reactions to be hosted in the future studies, the monolith length is extensible to make it compatible with the reaction characteristic times. The monolith section is connected to an upstream packed bed (length 300 mm; sphere diameter 10 mm) which serves as distributor. In addition, a packed-bed section (length 100 mm; sphere diameter 10 mm) is hyphenated downstream to the monolith section. In the present study, the global assemblage of the three sections is taken into account. This low column-to-particle-ratio is chosen as the base condition as it reflects an experimental setup representative of that studied by Ding et al.[7,8] Larger ratios could run the risk of inducing depth filtration and capture of particles in the pre- and postdistributors, which may not be desirable. As a first approximation, a two-dimensional symmetric domain is considered, providing a simplified scenario to get insight into the packed-bed-induced maldistribution flow characteristics in monolithic structured reactor. The computational geometry is schematically shown in Figure 3.

Table 1. Basic Simulation Conditions Used in This Work

parameter	value
operation pressure (Pa)	1.1×10^5
gas phase (air)	
density (kg/m^3)	1.225
viscosity (kg/m·s)	1.7894×10^{-5}
inlet velocity (m/s)	2.14
solid phase (biomass particles)	
density (kg/m^3)	450.0
particle diameter (m)	55×10^{-6}
inlet velocity (m/s)	2.14
inlet solid volume fraction	6.4269×10^{-4}
upstream packed-bed section	
length (m)	0.300
column diameter (m)	0.050
particle diameter (m)	0.010
central monolith section	
length (m)	0.600
diameter (m)	0.050
channel size (m)	3.0×10^{-3}
pitch (m)	3.3×10^{-3}
downstream packed-bed section	
length (m)	0.100
column diameter (m)	0.050
particle diameter (m)	0.010

The solid volume fraction at the inlet is given by ref 13, assuming homogeneous flow

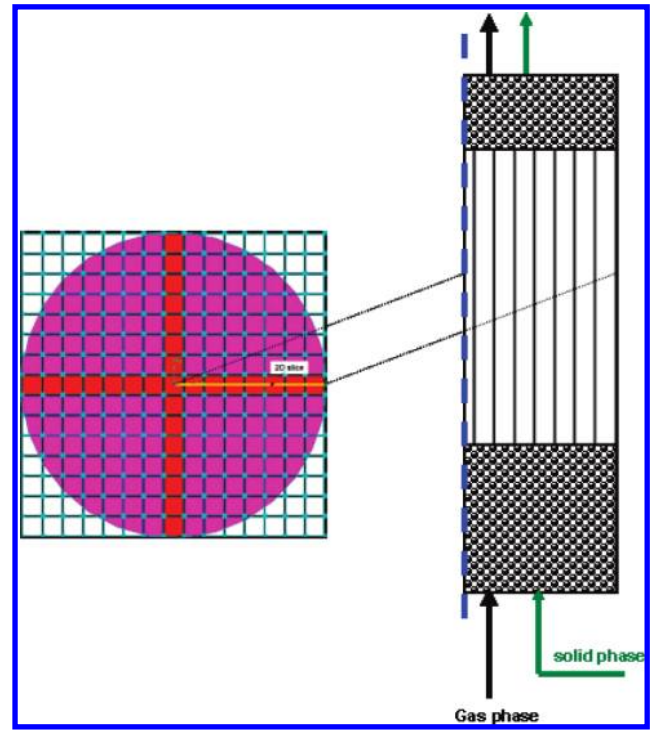

Figure 3. Two-dimensional computational geometry with the assemblage of three-section structured/nonstructured packings (yellow line, 2D symmetric plane).

$$a_s = \frac{G_s}{G_s + \rho_s U_g} \tag{23}$$

where U_g is the superficial gas velocity and G_s is the solids mass flux. Flat velocity profiles are set as inlet boundary conditions for gas and suspended phases, which are calculated as follows

$$u_s|_{z=0} = \frac{G_s}{\rho_s a_s} \tag{24}$$

$$u_g|_{z=0} = \frac{U_g}{(1 - a_s)} \tag{25}$$

where u_s is the axial interstitial solids velocity and u_g is the axial interstitial gas velocity. A no-slip condition is used for all the impermeable walls.

The model equations are solved in steady state using commercial software Fluent (version 6.3). The porosity distribution model and the interphase momentum exchanges are implemented via user defined functions. The second-order upwind scheme is used for the convection terms of momentum equations. The velocity−pressure coupling is treated using the SIMPLE algorithm.

6. Results and Discussion

In this work, an attempt is made to investigate gas−solid two-phase flows through the aforementioned composite monolith geometry. The gas continuous phase considered is air and the solid suspended phase is biomass particles. The size of solid particles is 55 μm. The basic simulation parameters used in this work are listed in Table 1.

6.1. Modeling of Two-Phase Flow Behavior in Monolith Structured Packings. Figure 4 shows the radial solid mass fluxes of the suspended phase in different packing sections (z (m) < 0 lower packed bed; 0 < z < 0.6 monolith block; z > 0.6 upper packed bed). It can be seen that the suspended particles are distributed unevenly across the monolith assemblage cross-section. The highest biomass solids flux takes place at r = 0.0165 m, i.e., 0.66 × column radius. It is very close to the value reported experimentally by Ding et al.[8] for glass beads using a positron emission particle tracking technique. In their work, it was found that the dominant peak of solid concentration occurs in the annular region around $r/R \approx 0.7$. Although the suspended particles (biomass particles) used in this simulation differ from those used by Ding et al.,[8] it can be conservatively concluded that the model has the ability to capture nonuniform distribution features of solid phase flow in monolithic structured packing, definitely within what may be regarded as qualitative approximations. In addition, it can also be seen that for the packed-bed sections, there is a dominant peak at a position close to the wall, which corresponds to a main feature of the measurement in gas−solid flow through packed bed.[23,24] This suggests that our model can be used to capture the main features from the experimental findings.

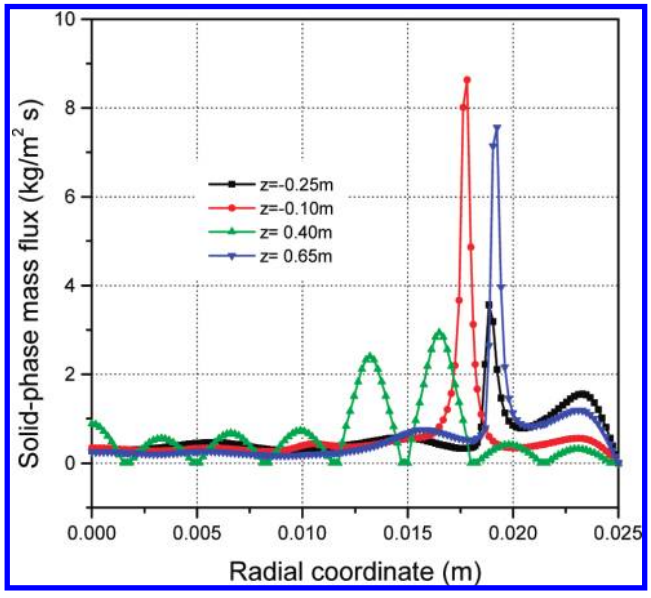

Figure 4. Solids biomass flux of suspended phase in different packing sections.

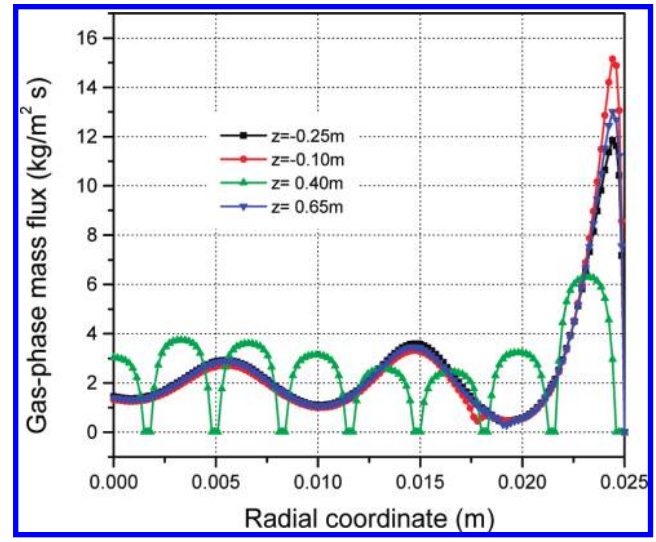

Figure 5. Gas mass fluxes mirroring Figure 4 simulations.

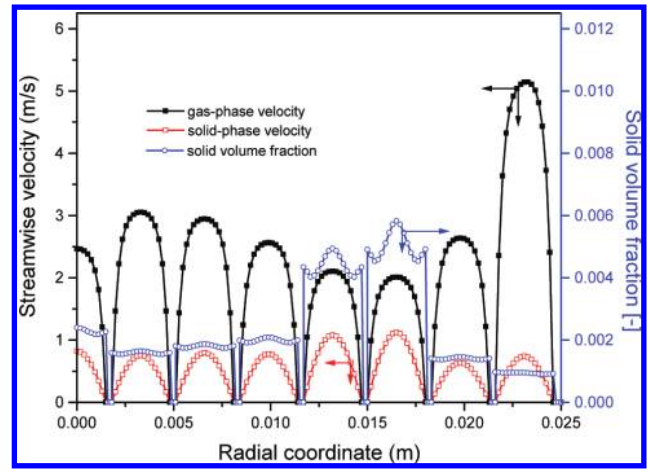

Figure 6. Channel dependence of gas-phase velocity, solid velocity, and solid holdup (z = 0.4 m).

Figure 5 shows the gas mass fluxes in different packing sections. It is shown that there exists a very strong near-wall channeling for the gas flow in the lower fixed-bed random packing. Due to the block effect of monolith structured geometry and no-slip effect from wall, the packed-bed induced maldistribution for gas phase is reduced to a great extent in the monolith section. However, the gas-phase maldistribution in different channels is still remarkable. The channel adjacent to the column wall is responsible for significant transport of the gas phase.

Figure 6 compares the radial profiles at z = +0.4 m of solid and gas velocities as well as the variation of solid volume fractions inside the monolith channels. It can be seen that the

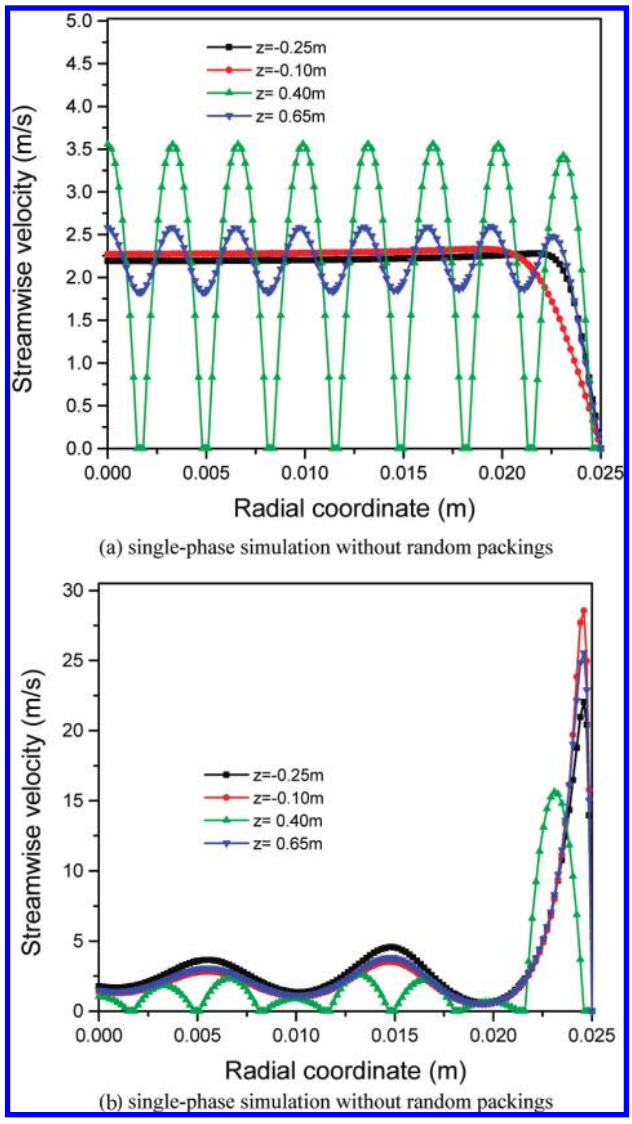

Figure 7. Gas-phase velocity in single-phase flow simulation. (a) Single-phase simulation without random packings. (b) Single-phase simulation with random packings.

nonuniform distribution characteristics for the gas and solid phases are completely different. The nonuniform distribution of the solid phase is evident, as reflected by both the solid velocity and the solid volume fraction. For the solids phase, the highest solid velocity can be found in two channels which are located two-channel away from the column wall. It is interesting to note that these two channels also correspond to the highest solid volume fraction, contributing to the largest solid transport capacity. It is also observed that the velocities of the gas phase are generally several times higher than those of the solid phase.

6.2. Comparison of Gas−Solid Two-Phase Flow with Single-Phase Flow. It is of interest to compare the two-phase and single-phase flow behaviors. For comparison purposes, two simulation cases for single-phase flow are considered in this work. In the first case, the random packing is not taken into account. That is, no packing is arranged in the upstream and downstream fixed-bed sections. In the second case, the packings in fixed-bed sections are enabled. Compared to the two-phase flow, the single-phase flow corresponds to a two-phase flow with zero solids volume fraction. Figure 7 shows the variation of gas-phase velocity with the radial coordinate at different axial locations. It can be seen from Figure 7a that, for disabled random

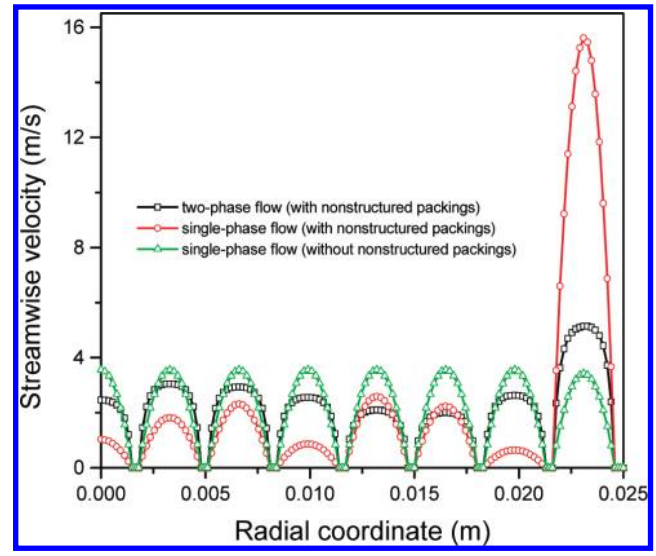

Figure 8. Comparison of gas-phase velocities under single-phase/two-phase simulation conditions (z = 0.4 m) with and without the nonstructured distributors.

packings (empty pipe), the distribution of gas velocity in the monolithic channels is almost uniform. However, when the empty parts of the upstream and downstream sections are packed with nonstructured packings of spheres, uniformity is broken. As shown in Figure 7b, the monolith gas flow distribution is susceptible to the upstream maldistribution.

As a comparison, Figure 8 shows the gas-phase velocity profiles under single-phase and two-phase simulation conditions. From this figure, it seems that single-phase flow with random packings brings about most serious anisotropic characteristic of flow in the monolith channels. Further, the introduction of solids phase can mitigate seriousness of maldistribution to some degree; however, the problem of solids-phase induced flow distribution will arise (as shown in Figures 4 and 6). Compared to single- and two-phase flow with nonstructured packing, the disabled packings (empty pipe) offer much uniform distribution of gas-phase flow in the monolith channels, except for some maldistribution in the channel closest to the column wall due to the empty pipe velocity profile.

6.3. Effect of Downstream-Section Packing on Flow Distribution in Monolith. It is also of interest to investigate whether or not the downstream-section packing mode has any noticeable impact on flow distribution in monolith section. In this work, comparative simulations have been performed to examine three different cases with different packing modes for the downstream section. The first case is default one in which the downstream section is packed with particles of 10 mm in diameter. The second case is a null packing (empty pipe) which allows the clear fluids to pass in this section. The last case corresponds to a nonhomogeneous composite packing mode. In this case, while maintaining the larger packed particles (diameter = 10 mm) in the upstream section, smaller particles of 5.0 mm in diameter are considered in the downstream-section packing, being entailed with higher flow resistance as opposed to the aforementioned two cases. It is noted here that in all these cases the upstream packing modes are kept same (i.e., randomly packed with 10 mm-in-diameter particles). Figure 9 shows the detailed comparison between the three packing modes for the gas and suspended solid phases. As in Figure 9a, there are some appreciable differences in gas velocities of the three cases for the two channels near the column wall.

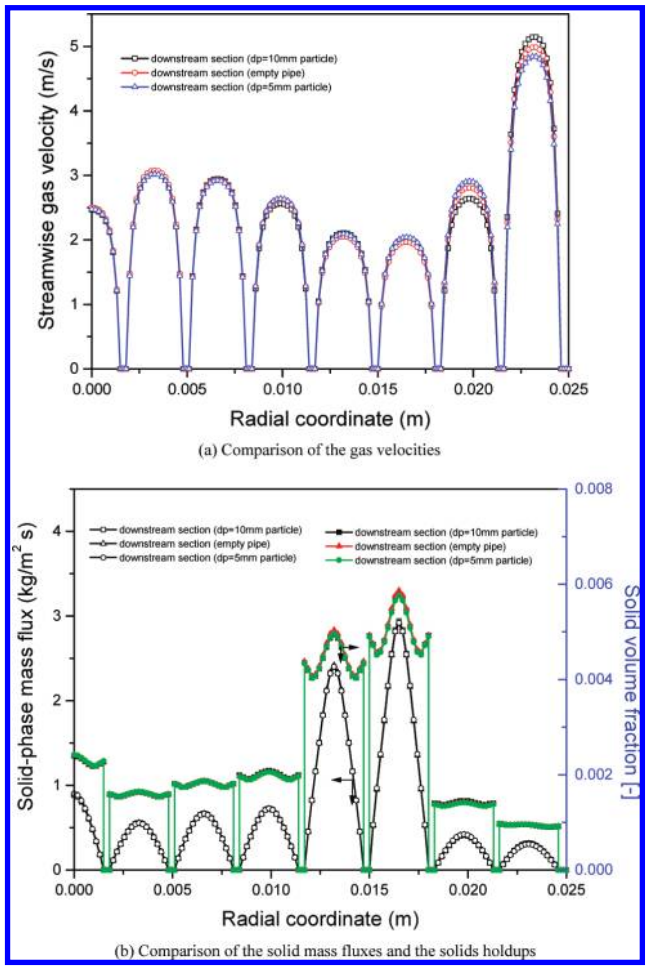

Figure 9. Comparison of monolith-section flow distribution characteristics ($z = 0.4$ m) with and without the nonstructured packing in the downstream section. (a) Comparison of the gas velocities. (b) Comparison of the solid mass fluxes and the solids holdups.

However, the overall change of gas velocities for the whole multichannel system is generally insignificant. In addition, the comparison of solid-phase mass fluxes and solids dynamic holdups is further performed. Figure 9b depicts a fairly high degree of matching of solids flow distribution characteristic between the three cases. These simulated results indicate that the effect of downstream-section packing mode on monolith maldistribution characteristics is generally negligible under our simulation conditions.

6.4. Effect of Particle Size of Random Packings on Flow Characteristics in Monolith. The size of the particles in the packed-bed sections affects not only the near-wall channeling phenomena but also the pressure drop of the reactor system. To reasonably select the particle sizes for a composite monolith, the effect of particle size in the nonstructured (random) packing sections on the flow characteristic in monolith section needs to be investigated. In this section, the influence of particle size of nonstructured (random) packings on the monolith maldistribution characteristic and the pressure drop is systematically investigated. In our simulation, two scenarios characterized by nonuniform and uniform radial porosity distributions are taken into account, as shown in Table 2. For the nonuniform porosity scenario, the radial porosity distribution is assessed by Mueller's correlation and three particle sizes (diameter = 10, 5.0, and 2.5 mm) are considered to be packed in the upstream and downstream sections. Here, the three simulation cases are referred to as Dp10_Mueller, Dp5.0_Mueller, and Dp2.5_Mueller for brevity (referring to Table 2). In the uniform porosity scenario, a mean porosity is used as input, which is determined by averaging the radial porosity distribution based on Mueller's correlation (for $d_p = 10$ mm). To further gain insight into the contributing mechanisms in interphase momentum interactions, the inclusion and exclusion of the phase interactions between the stationary packing and the flowing solids (or gas) phase are considered here for decoupling the effect of various contributing mechanisms. As in Table 2, three simulation cases (labeled as Dp10_G1S1, Dp10_G1S0, and Dp10_G0S0) are considered for the uniform-porosity scenario. It is noted here that the numbers "1" and "0" denote inclusion and exclusion, respectively. And, "G" and "S" denote interphase interaction between gas phase and packed phase and interphase interaction between suspended solid phase and packed phase, respectively.

Table 2 presents the detailed comparison of pressure drop and flow maldistribution in monolithic channels for the two scenarios (nonuniform radial porosity distribution and uniform radial porosity distribution). As shown in this table, the pressure drop contributions from different packing sections, the monolith maldistribution factor, and flow factors for each phase are calculated and presented as performance metrics. The relevant details of the channel locations and the centerline-based pressure sampling in the three-section monolith system are graphically illustrated in Figure 10. The effect of particle size is evaluated in case of nonuniform radial porosity distribution. It can be seen from Table 2 that the reduction of particle size results in the increase of bed pressure drops in the upstream and downstream packed sections, as expected. The pressure drop in the monolith section is found to increase as the particle size decreases. Due to the near wall channeling, the differences in pressure drop between the near-wall region and the bulk region can be observed in the three packing sections. These differences are magnified in case of employing packed particle of larger size, corresponding to the lower column-to-particle ratio. The decrease of particle size will bring a positive contribution to the improvement of the overall flow maldistribution for the gas phase, as indicated by the decreasing trend in gas-phase maldistribution factor. The gas-phase flow factors in monolith channels demonstrate specifically the contribution of reducing particle size in suppressing the severity of the near-wall channeling. As compared to the gas phase, the effect of decreasing particle size on the maldistribution behavior is not so evident for the solid phase. With decreasing the particle size, the value of solid-phase maldistribution factor increases first and then decreases again, showing a nonlinear variation relationship. The solid-phase flow factors in monolith channels also disclose the details of the nonlinear change, including both the change in peak magnitude and the migration in peak location. Note that reduction in particle size in the upstream and downstream packed beds would increase the risk for these sections to plug with biomass particles. Since the filtration ability of the beds was not included in the model analysis, it is believed that smaller particle beds would exhibit different maldistribution behaviors as the permeability of the bed could evolve with biomass particle capture.

Averaging the radial porosity distribution of the Dp10_Mueller case leads to a mean porosity value of 0.444, which is used as the input of porosity for the uniform-radial-porosity simulation cases (Dp10_G1S1, Dp10_G1S0, and Dp10_G0S0). It is interesting to make a direct comparison between the Dp10_G1S1 and Dp10_Mueller simulation cases. In practice, the two cases

Table 2. Effect of Particle Size and Radial Porosity Distribution of Nonstructured Packings on the Flow Characteristics in Monolith

	nonuniform radial porosity distribution			uniform radial porosity distribution			
	Dp10_Mueller	Dp5.0_Mueller	Dp2.5_Mueller	Dp10_G1S1	Dp10_G1S0	Dp10_G0S0	empty pipe
			pressure drop (Pa/m)				
average pressure drop[a]							
upstream section	−5143.8	−15417.1	−42157.9	−7065.4	−6481.3	−23.8	−24.2
monolith section	−750.8	−770.2	−949.8	−855.4	−856.9	−840.2	−840.2
downstream section	−5297.5	−15335.0	−42338.8	−7035.0	−6460.0	−31.3	−30.0
wall-adjacent pressure drop[a]							
upstream section	−4743.3	−15300.0	−42256.7	−7086.7	−6500.0	−36.7	−36.7
monolith section	−898.3	−831.7	−948.3	−843.3	−846.7	−835.0	−835.0
downstream section	−5100.0	−15360.0	−42380.0	−7060.0	−6480.0	−30.0	−30.0
			maldistribution factor				
solids phase	0.298	0.353	0.220	0.077	0.065	0.030	0.024
gas phase	0.121	0.109	0.080	0.031	0.027	0.009	0.007
			flow factor				
solids phase							
channel_00	0.822	0.729	0.760	0.973	1.006	1.052	1.062
channel_01	0.522	0.654	0.746	0.992	0.992	1.136	1.094
channel_02	0.628	0.653	0.731	0.992	1.005	1.058	1.008
channel_03	0.678	0.690	0.776	0.995	1.026	0.972	0.957
channel_04	2.122	1.072	0.976	1.018	1.099	0.931	0.958
channel_05	2.538	3.400	2.180	1.136	1.240	0.967	1.016
channel_06	0.388	0.602	1.639	1.338	1.041	1.021	1.028
channel_07	0.301	0.200	0.191	0.556	0.591	0.863	0.877
gas phase							
channel_00	0.865	0.896	0.956	0.997	0.990	0.989	0.985
channel_01	1.069	0.946	0.966	0.991	0.994	0.962	0.974
channel_02	1.034	0.965	0.969	0.991	0.991	0.983	1.000
channel_03	0.897	0.934	0.975	0.990	0.984	1.010	1.016
channel_04	0.735	0.815	0.928	0.983	0.963	1.023	1.014
channel_05	0.699	0.655	0.810	0.948	0.925	1.007	0.990
channel_06	0.913	1.098	0.858	0.899	0.976	0.985	0.983
channel_07	1.787	1.692	1.540	1.202	1.177	1.042	1.037

[a] These values are calculated/averaged using the multichannel centerline sampling data (see Figure 10 for the geometrical details).

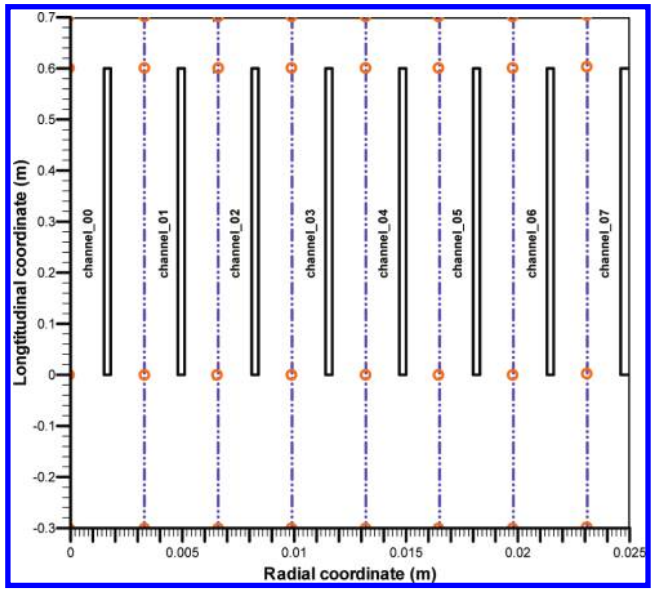

Figure 10. Details of the channel locations and centerline-based pressure sampling in the three-section monolith system.

represent different methodologies in treating the nonuniformity of radial porosity distribution. From a physical viewpoint, the latter takes into account the radial nonuniformity in porosity distribution while the former neglects this kind of nonuniformity by simplifying it as flat distribution. It can be seen in Table 2 that the Dp10_G1S1 simulation case with the uniform-radial-porosity assumption can render a remarkably improved flow distribution characteristics for both the phases, as opposed to its counterpart (Dp10_Mueller). However, judging from the distribution of two-phase flow factors, it is found that the near-wall higher loading transport for the gas-phase as well as the appearance of dominant peak in the solid-phase mass flux are still noticeable even in this ideal case. To get further insight into the phenomena, decoupling interphase interaction is attempted in this work to observe the evolutionary change in flow distribution. To this end, the additional simulation cases (Dp10_G1S0 and Dp10_G0S0) are introduced for comparison purpose. By comparing the three simulation cases, one may conclude that the interphase interaction mechanisms have an "incremental" contribution in affecting the flow maldistribution; and the gradual exclusions of the interphase interactions lead to improved flow distribution for both the phases. Finally, we present the global contour comparison of the solid-phase mass flux in the composite monolith for all these simulation cases (with/without considering nonuniformity in radial porosity distribution), as shown in Figure 11. The null-packing case (empty pipe) is also presented here. Comparing with Dp10_G0S0, the null-packing case can be regarded as a variant of Dp10_G0S0 with the porosity value of 1.0. As indicated in Figure 11, the nonuniformity of flow distribution in monolith structured packing section is to a great extent imprinted with the unique flow characteristics in the upstream nonstructured (random) packing section.

7. Conclusions

In the present work, a process concept for biomass gasification is first proposed which involves the hybridization of gasification/combustion reactions in a monolithic structured reactor by using high-temperature phase-change material to intensify the process heat management. Following the proposal of this concept, a

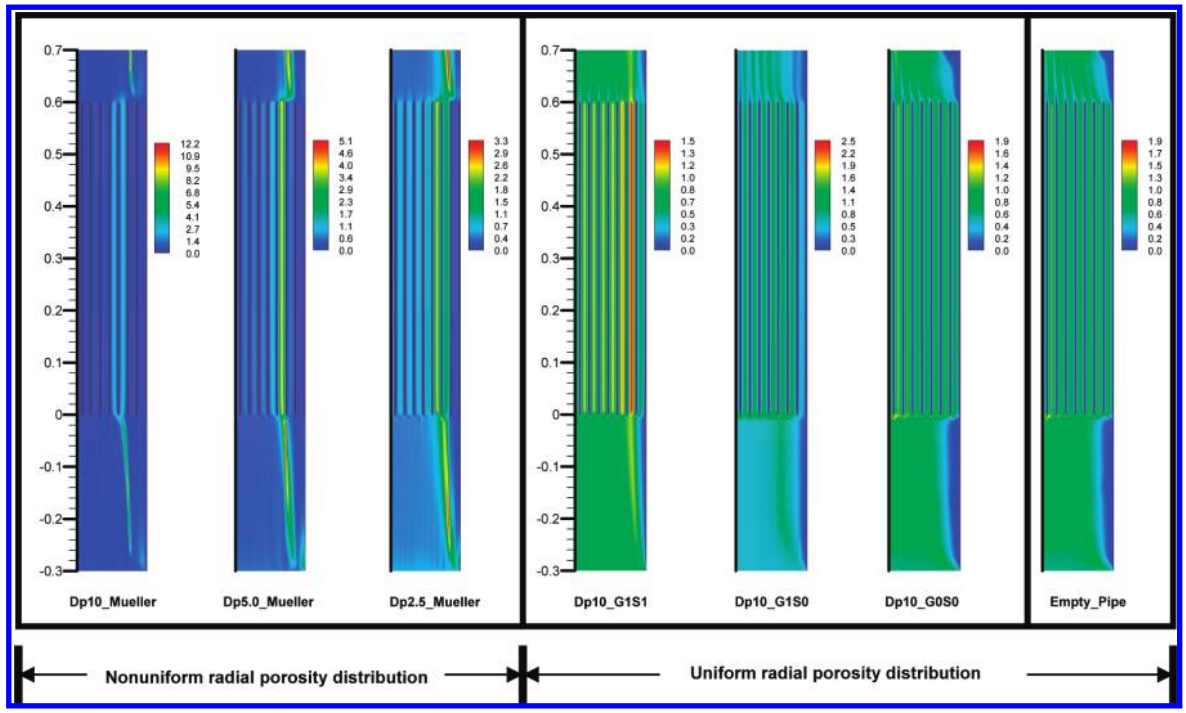

Figure 11. Effect of particle size and porosity radial distribution on the solid mass flux distribution in the composite monolith system.

computational fluid dynamics model is developed to investigate the gas−solid (biomass particles) two-phase flow distribution characteristics in monolithic structured packings. This model is based on Eulerian−Eulerian multifluid modeling approach with closure laws according to the kinetic theory of granular flow. An assemblage of monolithic structured packings with nonstructured packed-bed sections is fully considered in our simulations with a view to effectively characterizing the flow maldistribution. The nonstructured random packed-bed sections are treated as porous media by implementing the nonuniformity of radial porosity distribution and the interphase interactions through user defined functions (UDFs).

The numerical investigation was carried out to systematically explore the two-phase flow distribution in the three-section composite monolith system. The simulation results indicate that there exists a very strong near-wall channeling for the gas-phase flow in the fixed-bed random packings. The suspended particles are distributed unevenly across the monolith assemblage cross-section, and the highest biomass solids flux takes place at a dimensionless column radius ≈0.66. The effect of downstream-section packing modes on monolith maldistribution characteristics can be generally considered as negligible under our simulation conditions. The reduction of particle size in the nonstructured packing sections results in an increase of pressure drop in the monolith section. In addition, decreasing particle sizes leads to a positive improvement in the overall flow distribution for the gas phase and a nonlinear variation trend in flow maldistribution for the solid phase. Compared to the nonuniform-radial-porosity assumption, the uniform-radial-porosity assumption provides considerably improved flow distribution characteristics for both the gas and solid phases. The interphase interaction mechanisms are found to exhibit "incremental" contributions in affecting the flow maldistribution. Gradual exclusion of the interphase interactions leads to an improved flow distribution for both the phases. The nonuniformity of flow distribution in monolith structured packing section is shown to be imprinted to a great extent with the unique flow characteristics in the upstream nonstructured packing section. The simulation results indicate the ability of CFD models to capture the nonuniformities of the flow pattern in monolithic structured packing, which we believe will further aid our development of the process concept.

Acknowledgment

Financial support from the "Chaire de recherche du Canada en procédés et matériaux pour des énergies durables" of the Natural Sciences and Engineering Research Council (NSERC) is gratefully acknowledged.

Nomenclature

a = constant in eqs 1a−1d
a_g = volume fraction of phase g
a_q = volume fraction of phase q
a_s = volume fraction of phase s
b = constant in eqs 1a−1d or coefficient in turbulence model
C_D = drag coefficient
d_p = diameter of packed particle, m
d_s = diameter of suspended particle, m
D = diameter of column, m
D^* = hydraulic diameter of a packed bed, m
e_{ss} = restitution coefficient of particle collisions
f_k = interaction coefficient between suspended phase and packed particles
Fr = Froude number
$\vec{g}$ = gravitational constant, m^2/s
g_0 = radial distribution function of interparticle collisions
G_s = flux of suspended phase, kg/m^2 s
I = unit tensor
I_{2D} = second invariant of the deviatoric stress tensor
J_0 = zeroth-order Bessel function
k_{θ_s} = diffusion coefficient for granular energy, kg/s·m
$\dot{m}_{i,0}$ = theoretical uniform flowrate of the qth phase in the ith channel, kg/s
$\dot{m}_i^q$ = realistic mass flowrate of the qth phase in the ith channel, kg/s
M_f^q = maldistribution factor of the qth phase in the ith channel

N_{ch} = number of channels
N_q = number of phases
p = fluid pressure, N/m^2
p_s = solid pressure, N/m^2
r = radial coordinate, m
r^* = dimensionless radial coordinate, [−]
Re_s = relative Reynolds number
S_g = source term due to gas−packing interaction
S_s = source term due to particulate−packing interaction
t = time, s
u_g = axial interstitial gas velocity at the inlet, m/s
u_s = axial interstitial solids velocity at the inlet, m/s
$\vec{U}_s$ = superficial suspended solids velocity vector
U_g = superficial gas velocity
$\vec{v}_g$ = velocity of gas phase, m/s
$\vec{v}_q$ = velocity of phase q, m/s
$\vec{v}_s$ = velocity of solid phase, m/s
v_s' = particulate fluctuating velocity, m/s

Greek Letters

β = combined coefficient of interphase momentum exchange, kg/m^3·s
β_{gs} = coefficient of interphase momentum exchange, kg/m^3·s
β_{Ergun} = fluid−solid interaction coefficient of the Ergun equation, kg/m^3·s
β_{Wen-Yu} = fluid−solid interaction coefficient of the Wen−Yu equation, kg/m^3·s
ε = voidage of packed bed
ε_B = constant in eqs 1a−1d
φ_{gs} = switch function
γ_{θ_s} = collisional dissipation of energy, kg/s^3·m
Γ_i^q = flow factor of the qth phase in the ith channel
λ_s = bulk viscosity of solid phase, Pa s
μ_g = shear viscosity of gas phase, Pa s
μ_s = shear viscosity of solid phase, Pa s
θ_s = granular temperature, m^2/s^2
ρ_g = density of phase g, kg/m^3
ρ_q = density of phase q, kg/m^3
ρ_s = density of phase s, kg/m^3
$\bar{\bar{\tau}}_g$ = gas stress tensor, N/m^2
$\bar{\bar{\tau}}_s$ = solid stress tensor, N/m^2

Subscripts

g = gas phase
i = ith channel
q = qth phase
s = solid suspended phase

Literature Cited

(1) Kobayashi, N.; Guilin, P.; Kobayashi, J.; et al. A new pulverized biomass utilization technology. *Powder Technol.* **2008**, *180* (3), 272–283.

(2) Florin, N. H.; Harris, A. T. Enhanced hydrogen production from biomass with in situ carbon dioxide capture using calcium oxide sorbents. *Chem. Eng. Sci.* **2008**, *63* (2), 287–316.

(3) Levenspiel, O. What will come after petroleum. *Ind. Eng. Chem. Res.* **2005**, *44* (14), 5073–5078.

(4) Pletka, R.; Brown, R. C.; Smeenk, J. Indirectly heated biomass gasification using a latent heat ballast. 1: experimental evaluations. *Biomass Bioenergy* **2001**, *20* (4), 297–305.

(5) Pletka, R.; Brown, R. C.; Smeenk, J. Indirectly heated biomass gasification using a latent heat ballast. Part 2: modeling. *Biomass Bioenergy* **2001**, *20* (4), 307–315.

(6) Potic, B.; Kersten, S. R. A.; Ye, M.; et al. Fluidization with hot compressed water in micro-reactors. *Chem. Eng. Sci.* **2005**, *60* (22), 5982–5990.

(7) Ding, Y. L.; Wang, Z. L.; Wen, D. S.; Ghadiri, M. Vertical upward flow of gas-solid two-phase mixtures through monolith channels. *Powder Technol.* **2005**, *153* (1), 51–58.

(8) Ding, Y. L.; Wang, Z. L.; Wen, D. S.; Ghadiri, M.; Fan, X. F.; Parker, D. Solids behavior in a dilute gas-solid two-phase mixture flowing through monolith channels. *Chem. Eng. Sci.* **2006**, *61* (5), 1561–1570.

(9) Mueller, G. E. Radial void fraction distributions in randomly packed fixed beds of uniformly sized spheres in cylindrical containers. *Powder Technol.* **1992**, *72*, 269–275.

(10) Giese, M.; Rottschafer, K.; Vortmeyer, D. Measured and modeled superficial flow profiles in packed beds with liquid flow. *AIChE J.* **1998**, *44* (2), 484–490.

(11) Lun, C. K. K.; Savage, S. B.; Jeffrey, D. J.; Chepurniy, N. Kinetic theories for granular flow: inelastic particles in Couette flow and slightly inelastic particles in a general flow field. *J. Fluid Mech.* **1984**, *140*, 223–256.

(12) Gidaspow, D.; Bezbaruah, R.; Ding, J. Hydrodynamics of circulating fluidized beds, kinetic theory approach. In *Fluidization VII, Proceedings of the 7th Engineering Foundation Conference on Fluidization*, New York; Potter, O. E., Nicklin, D. J., Eds.; Engineering Foundation, 1992; pp 75−82.

(13) Gidaspow, D., *Multiphase Flow and Fluidization: Continuum and Kinetic Theory Descriptions*; Academic Press: New York, 1994.

(14) Wen, C. Y.; Yu, Y. H. A generalized method for predicting minimum fluidization velocity. *AIChE J.* **1966**, *12* (3), 610.

(15) Ergun, S. Fluid flow through packed columns. *Chem. Eng. Prog.* **1952**, *48* (2), 89–94.

(16) Yamaoka, H. Mechanisms of hanging caused by dust in a shaft furnace. *ISIJ Int.* **1991**, *31*, 939–946.

(17) Shibata, K.; Shimizu, M.; Inaba, S. Pressure loss and hold up powders for gas-powder two phase flow in packed beds. *ISIJ Int.* **1991**, *31*, 434–439.

(18) Van der Ham, A. G. J.; Prins, W.; Van Swaaij, W. P. M. Hydrodynamics of a pilot-plant scale regularly packed circulating fluidized bed. *AIChE Symp. Ser.* **1993**, *89*, 53–72.

(19) Dong, X. F.; Zhang, S. J.; Pinson, D.; et al. Gas-powder flow and powder accumulation in a packed bed: II-numerical study. *Powder Technol.* **2004**, *149*, 10–22.

(20) Boremans, D.; Rode, S.; Wild, G. Liquid flow distribution and particle-fluid heat transfer in trickle-bed reactors: the influence of periodic operation. *Chem. Eng. Process.* **2004**, *43*, 1403–1410.

(21) Hoek, P. J.; Wesseling, J. A.; Zuiderweg, F. J. Small scale and large scale liquid maldistribution in packed columns. *Chem. Eng. Res. Des.* **1986**, *64*, 431–449.

(22) Marcandelli, C.; Wild, G.; Lamine, A. S.; Bernard, J. R. Liquid distribution in trickle-bed reactors, oil and gas science and technology. *Rev. IFP* **2000**, *55* 407−415.

(23) Ding, Y. L.; Wang, Z. L.; Wen, D. S.; Ghadiri, M.; Fan, X. F.; Parker, D. Solids behaviour in a gas-solid two-phase mixture flowing through a packed particle bed. *Chem. Eng. Sci.* **2005**, *60* (19), 5231–5239.

(24) Li, S. Q.; Ding, Y. L.; Wen, D. S.; He, Y. Modelling of the behaviour of gas-solid two-phase mixtures flowing through packed beds. *Chem. Eng. Sci.* **2006**, *61* (6), 1922–1931.

Received for review August 6, 2008
Revised manuscript received October 16, 2008
Accepted October 17, 2008

IE8012083